Article

Cite This: Biomacromolecules 2019, 20, 693−704

pubs.acs.org/Biomac

Strong, Ductile, and Waterproof Cellulose Nanofibril Composite Films with Colloidal Lignin Particles

Muhammad Farooq, Tao Zou, Guillaume Riviere, Mika H. Sipponen,* and Monika Österberg*

Aalto University, School of Chemical Engineering, Department of Bioproducts and Biosystems, Vuorimiehentie 1, 02150 Espoo, Finland

Supporting Information

ABSTRACT: Brittleness has hindered commercialization of cellulose nanofibril (CNF) films. The use of synthetic polymers and plasticizers is a known detour that impairs biodegradability and carbon footprint of the product. Herein, we utilize a variety of softwood Kraft lignin morphologies to obtain strong and ductile CNF nanocomposite films. An optimum 10 wt % content of colloidal lignin particles (CLPs) produced films with nearly double the toughness compared to a CNF film without lignin. CLPs rendered the films waterproof, provided antioxidant activity and UV-shielding with better visible light transmittance than obtained with irregular lignin aggregates. We conclude based on electron microscopy, dynamic water sorption analysis, and tp-DSC that homogeneously distributed CLPs act as ball bearing lubricating and stress transferring agents in the CNF matrix. Overall, our results open new avenues for the utilization of lignin nanoparticles in biopolymer composites equipped with versatile functionalities for applications in food packaging, water purification, and biomedicine.

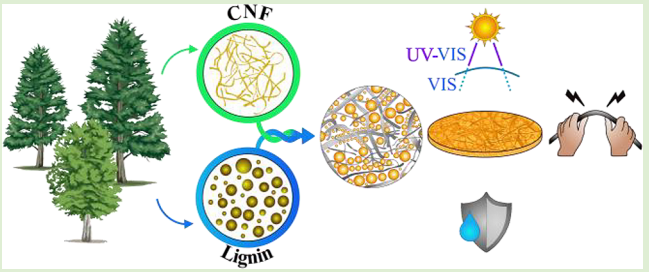

INTRODUCTION

Renewable plant biomass is a viable alternative to fossil carbon resources in the production of materials and chemicals. As contrasted to the production of platform chemicals from wood, it would appear more lucrative to isolate and use lignocellulosic biopolymers in their polymeric form with a lower energy penalty and moderate production cost. Fully biobased nanocomposites from renewable resources are next generation materials with untapped potential for replacing conventional petroleum-based composites in various applications such as biodegradable packaging for food and beverages, biomedical materials for wound dressings and as membranes in water treatment technology.[1,2] Important properties in the aforementioned applications include ductility and strength, UV-shielding, water resistance, tunable porosity, biocompatibility, and low cytotoxicity. Cellulose and lignin, the two major components in wood, qualify in most of these, making them ideal components of biobased nanocomposites. However, the inherent structural heterogeneity and brittleness of lignin and hydrophilicity of cellulose have to date obstructed their composite use, despite the synergistic coexistence of lignin and cellulose in plant cell walls.[1,3−5]

Wood ultrastructure reveals a laminar material consisting of strong cellulosic fibrils embedded in a lignin−hemicellulose matrix that dissipates fracture energy and hinders crack propagation.[6] This highly ordered, layered structure renders wood a tough composite. Although generally considered to be amphiphilic and not truly hydrophobic, lignin provides water resistance to the xylem that serves in the water transport in vascular plants.[7] It would therefore seem that the concentration of lignin in the cellulosic composite walls is central to the localized water impermeability of plant tissues.

Cellulose in the form of cellulose nanofibrils (CNF) disintegrated from wood has generated prevailing interest as an excellent natural fiber material due to its renewable availability, nontoxicity, and biodegradability.[8] CNF form films with high mechanical strength and stiffness, optical transmittance, low oxygen permeability, and low coefficient of thermal expansion.[9] However, the films are often brittle and various synthetic or natural polymers are added to increase ductility. The inherent role of lignin in providing strength and structural rigidity to plant cell walls would make it a logical choice as a reinforcing agent in nanocomposites. Nevertheless, data is lacking on the use of lignin in CNF-based composite films to mimic the natural composite structure of wood. One of the reasons could be the difficulty to disperse isolated lignin aggregates into the CNF matrix at the nanoscale. In addition, intrinsic heterogeneity of lignin structure, broad molecular weight distribution, and limited solubility with other polymeric systems restrict its use in high performance nanocomposites.[5]

Much more is known about (lignin-containing) films prepared from CNF that contains residual lignin.[10−13] While

Special Issue: The Rational Design of Multifunctional Renewable-Resourced Materials

Received: September 12, 2018
Revised: October 23, 2018
Published: October 25, 2018

DOI: 10.1021/acs.biomac.8b01364
Biomacromolecules 2019, 20, 693−704

Scheme 1. Preparation of CNF Film and CNF−Lignin Nanocomposite Films: (1) Blending of One of the Lignin Dispersion with CNF, (2) Film Formation by Pressure-Assisted Filtration, and (3) Ambient Drying under 5 kg Load or Hot Pressing at 100 °C[a]

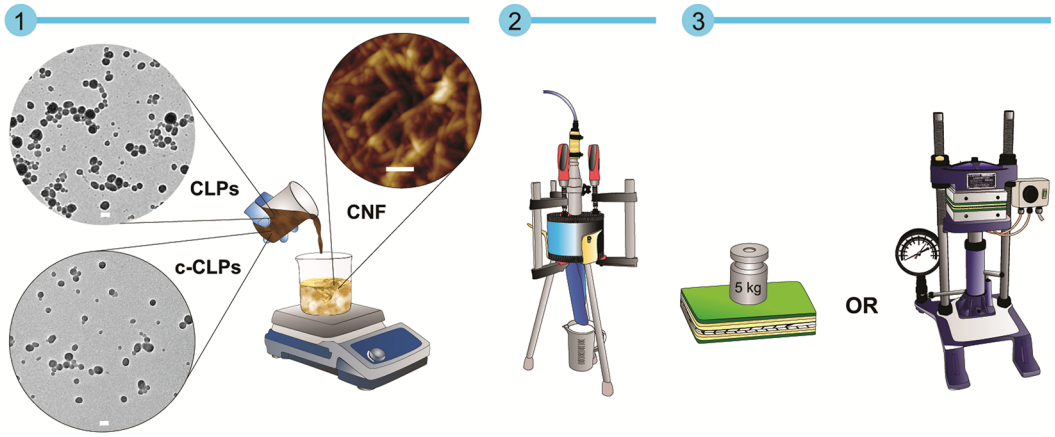

[a]Scale bars in TEM and AFM images: 100 nm.

Bian et al.[13] reported a decrease in mechanical properties due to residual lignin, Rojo et al.[11] showed that the tensile strength and elastic modulus of CNF films were not deteriorated at a residual lignin content up to 14%. Herrera et al.[12] concluded that heat treatment of the residual lignin-containing CNF films has a significant detrimental effect on the mechanical properties. However, it is difficult to conclude about the effect of lignin concentration, independent of the differences in the pulping conditions and consequential physicochemical modifications in the residual lignin.

Colloidal lignin particles (CLPs) have a well-defined surface chemistry and are easy to disperse in aqueous media. Due to the abundance of hydroxyl groups on their surface it is possible that the CLPs do not disrupt the hydrogen bonding pattern in the CNF network as much as many of the previously employed synthetic polymers.[14] Despite the recent advances in the scalable production of CLPs[15] and versatile new applications,[16−19] the potential of spherical lignin particles to enhance the properties of cellulosic nanocomposites is largely unexplored. In a very recent study, Liu demonstrated the positive effect of in situ formed lignin nanoparticles on the mechanical properties of nanocomposites.[20] However, the radical scavenging, UV-shielding capacity, and water resistance of lignin−CNF nanocomposite films have remained elusive.

In the present work, we compare the promising features of CNF, CLPs, cationic lignin solution, cationic CLPs (c-CLPs), and bulk softwood Kraft lignin in nanocomposite films. We show that at optimal lignin concentration, the nanocomposites demonstrate tougher film structure along with the highest strain at failure values reported thus far for all-lignocellulose films. Moreover, we show that the incorporation of CLPs renders the nanocomposite films waterproof, while exhibiting complementary UV shielding and radical scavenging capability. We discuss the importance of controlling drying conditions and lignin morphology in the preparation of the nanocomposites. Achieving the aforementioned combination of properties using the two most abundant wood polymers presents new opportunities in the field of green biobased nanocomposites for food packaging, water purification, and biomedical applications.

EXPERIMENTAL SECTION

Materials. Softwood Kraft lignin (BioPiva 100) isolated using the LignoBoost process at Domtar's Plymouth plant (NC, U.S.A.) was utilized in this work. The characterization of this lignin have been performed previously by us.[16] All chemicals and solvents were purchased from Sigma-Aldrich and VWR and were used without any further purification. The preparation of cellulose nanofibrils (CNF) was described by Österberg et al.[1] In brief, never dried bleached hardwood Kraft pulp fibers were washed into sodium form, and subjected to mechanical disintegration. Fibrillation was performed by using a type M-110P microfluidizer (Microfluidics, Newton, Massachusetts, U.S.A.) by a single pass through a series of 400 and 200 μm chambers, followed by six passes through a series of 400 and 100 μm chambers. The operating pressure was 2000 bar. The resulting CNF suspension of 2 wt % solid content was stored at 4 °C until use. The raw material and the fibrillation method were the same as previously used, so we expect the fibrils to have an average width of 5−20 nm and length of several micrometers[1] and a ζ-potential around −3 mV.[21]

Preparation of Kraft Lignin Suspension. A known concentration of Kraft lignin was suspended in deionized water using an IKA T18 basic ULTRA-TURRAX device at speed 5 for 1 min. Following the homogenization, the lignin suspension was used within 1 h for the preparation of CNF−lignin films.

Preparation of Water-Soluble Cationic Lignin. Cationic lignin used in this work originated from the same batch as previously described and characterized.[17] The synthesis procedure included reacting Kraft lignin (2.5 g dry basis) in aqueous 0.2 M NaOH with 0.5 g of glycidyltrimethylammonium chloride at 70 °C during 1 h. Upon completion of the reaction, the mixture was neutralized to pH 7. Purification of the resultant suspension was performed by dialysis in a 1 kDa MWCO Spectra/Por 7 tubing (Spectrum Laboratories) against deionized water. After centrifugation of the dialyzed suspension, the soluble fraction of cationic lignin (Catlig) at pH 7 was obtained at a mass yield of 55%.

Preparation of Colloidal Lignin Particles. The preparation of colloidal lignin particles was initiated by dissolving 5.00 g of softwood Kraft lignin (dry basis) in 500 mL of acetone/water 3:1, v/v. The solution was stirred for 3 h at room temperature, followed by filtrating using a glass microfiber filter (Whatman GF/F, pore size 0.7 μm) to remove undissolved solids. The obtained solution was rapidly poured into 1000 g of vigorously stirred deionized water. Acetone was removed by evaporation under reduced pressure at 40 °C to obtain the CLP dispersions used in this work (0.5 and 1.0 wt %). The mass yield of the colloidal lignin particles (CLPs) was 88%.

DOI: 10.1021/acs.biomac.8b01364
Biomacromolecules 2019, 20, 693−704

Preparation of Cationic Colloidal Lignin Particles. The preparation of cationic lignin particles (c-CLPs) was achieved by adding CLP dispersion slowly into vigorously stirred aqueous cationic lignin solution.[17] Cationic lignin solution was adjusted to pH 4 with 0.1 M HCl prior to the addition of CLP dispersion. c-CLPs at five different Catlig to CLPs dry weight ratios, 50, 100, 150, 200, and 300 mg g^{-1} were prepared.

Particle Size and ζ-Potential Analysis of CLPs and c-CLPs. The size distribution and ζ-potentials of CLP and c-CLP dispersions and Kraft lignin suspension were analyzed using a Zetasizer Nano ZS90 instrument (Malvern Instruments Ltd., U.K.). A dip cell probe was utilized for the determination of the ζ-potential. Mean values of three replicates of *Z*-average particle diameter and ζ-potential were used in the analysis and reporting of data.

Film Preparation. CNF films and lignin−CNF nanocomposite films were prepared according to the procedure reported by Österberg et al.[1] with a slight modification. The CNF suspension was diluted to 0.8 wt % solid content in deionized water and stirred for 2 h for pure CNF films or mixed with lignin suspension or solution prior to filtration. The lignin content was 0, 2, 5, 10, 20, and 50 wt % of the total dry weight in the CNF−lignin suspension. The mixture was stirred gently for 15 min, followed by filtration at 2.5 bar over pressure for 45 min over a 10 μm pore size open mesh Sefar Nitex polyamine monofilament fabric, placed on the top of a VWR grade 415 filter paper. The wet films obtained were ambient dried at 23 °C and 50% relative humidity (RH) for 72 h under a load of 5 kg. For comparison, Carver Laboratory press (Fred S. Carver Inc.) was used to prepare hot pressed (HP) films at 100 °C and 1800 Pa for 90 min. The obtained films were stored at 23 °C and 50% RH before testing. Filtrates were collected from each film preparation to determine gravimetrically the filtration process efficiency. The nanocomposites films prepared from pure CNF are referred as CNF, while the nanocomposite films prepared incorporating cationic colloidal lignin particles, colloidal lignin particles, soluble cationic lignin and Kraft lignin are termed c-CLP, CLP, Catlig, and KL, respectively. Table S1 shows composition and mass balance closure (98−100%) for each nanocomposite, while the overall film preparation process is illustrated in Scheme 1.

Tensile Testing. Mechanical properties of the CNF-based films were analyzed by measuring the tensile stress and strain at break with a universal testing machine (Instron 4204, U.S.A.) equipped with a 100 N load cell. The rectangular film specimens of 50 × 5 mm^2 with known thickness were conditioned for 48 h and subjected to 2 mm min^{-1} strain in the measurement environment of 50% RH at 23 °C. The sample edges were glued onto a paper frame in order to avoid slippage in the tensile grips. Young's modulus (*E*) was determined from the slope in the initial linear region of the stress−strain curve and tensile toughness was calculated by integrating the area underneath the stress−strain curve. The results are reported as mean value ± one standard deviation of a minimum of seven samples.

Microstructure Analysis Using FESEM and TEM. The surface and cross-sectional morphological characterization of CNF and lignin−CNF nanocomposite films was studied using a Zeiss Sigma field emission scanning electron microscope (FESEM; Zeiss Sigma VP, Germany). To examine the surface morphological features, film samples were imaged attached onto carbon tape. For bulk morphological characterization, fractured surfaces generated from tensile testing were utilized. The samples were sputter-coated with iridium using Agar high-resolution sputter coater to deposit an iridium layer of 3 nm. Micrographs of surface and cross-section morphologies were acquired at the accelerating voltage of 3 or 1.5 kV using a secondary electron detector and a working distance of 3−5 mm. Fiji ImageJ software (Research Services Branch, NIH, Bethesda, Maryland, U.S.A.) was used for the image analysis. For transmission electron microscopy (TEM), dispersions of CLPs and c-CLPs were deposited on carbon square mesh grids and dried under ambient conditions. TEM images were acquired in bright-field mode on a FEI Tecnai 12 operating at 120 kV.

Dynamic Vapor Sorption (DVS). A dynamic gravimetric water sorption analyzer (DVS Intrinsic, U.K.) was used to investigate the water sorption capacity of CNF-based nanofilms. A sample of up to 15 mg was placed in the sample pan and then weighed with an accuracy of 0.1 μg. The measurements were made at 25 °C. The RH was set to increase from 0% to 95% in 20 steps and then decrease to 0%. At every target humidity stage, the RH was kept constant until the rate of sample mass change was less than 0.001% min^{-1}, before proceeding to the next increment. The following equation was utilized to calculate the moisture uptake of each sample:

$$\text{moisture uptake} = 100 \times \frac{W_{\text{moist}} - W_{\text{dry}}}{W_{\text{dry}}}$$

where W_{moist} is the weight of the sample equilibrated at certain RH% and W_{dry} is the dry sample weight at 0 RH%.

DSC Thermoporometry. The pore size distribution of the CNF film and lignin-containing CNF nanocomposite films was evaluated by using DSC-thermoporometry (tp-DSC) adopted from Park et al.[22] and using the published temperature program as shown in Table S2.[23] Thermoporometry is based on the freezing point depression of water confined in pores, with melting point increasing as the pore diameter increases. For tp-DSC, circular samples of 5 mm in diameter (1.3−2.0 mg) were submerged overnight in deionized water for complete wetting. Wetted samples were placed in 50 μL preweighed aluminum pans and were sealed using a pan crimper press. Duplicate measurements were carried out on DSC 6000 (PerkinElmer, U.S.A.) equipped with a cooling apparatus under 20 mL min^{-1} nitrogen gas flow.

Water Permeability. Water permeability of CNF film and lignin−CNF nanocomposite films was tested under ambient pressure and in suction filtration (full water flow suction). In each of the experiments, 100 mL of deionized (MQ) water was added into the Millipore filtration funnel, and the amount of water permeated through the nanocomposite film was weighed at time intervals.

Stability in Physiological Buffer Medium. Stability of the films was determined in aqueous buffer medium, simulating physiological conditions. Circles cut from the films were weighed into 2 mL microcentrifuge tubes and immersed in 1.5 mL of 0.5× PBS buffer (pH 5.5). After 24 h of continuous mixing in the carousel rotator at 37 °C, the absorbance readings were recorded at 280 nm to evaluate leaching of lignin.

Optical properties and antioxidant activity. Transmittance of the films obtained at different conditions were recorded on a UV−vis spectrophotometer (Shimadzu UV-2550). The average thickness of the films was 85 μm. The antioxidant assay reported by Re et al.[24] was adapted with a few modifications to enable analysis of insoluble films using tannic acid for calibration. Freshly prepared $ABTS^{\bullet+}$ radical cation stock solution was diluted in water until reaching an absorbance of 0.6 at 734 nm at 25 °C before each series of measurements. Circular specimens of films (1−4 mg) were mixed with 2 mL of $ABTS^{\bullet+}$ radical cation solution at 25 °C using a Stuart tube rotator SB2. For calibration, 20 μL aqueous tannic acid in the range of 0.02−0.50 mg mL^{-1} was added into 2 mL of $ABTS^{\bullet+}$ radical cation solution. The absorbance at 734 nm was measured at 25 °C exactly 1 h after mixing of the components protected from light. Reduction of the absorbance was calculated relatively to the blank ($ABTS^{\bullet+}$ radical cation, 1 h after preparation). Films were analyzed in triplicates and standards in duplicates. Mean values were calculated and expressed as tannic acid equivalents (TAE) relative to the dry weight of the film sample, that is, mg of TAE g^{-1} of film.

RESULTS AND DISCUSSION

The objective of this work was to gain fundamental understanding of how morphology of lignin, that is, whether it is added as well-defined colloidal spheres or as lignin powder, surface charge, and lignin content affect the properties of CNF−lignin nanocomposites. The intention was to explore whether the combination of the two nanoscaled biomaterials could provide synergistic properties resembling those in plant cell walls. Our hypothesis was that we would be able to control

DOI: 10.1021/acs.biomac.8b01364
Biomacromolecules 2019, 20, 693−704

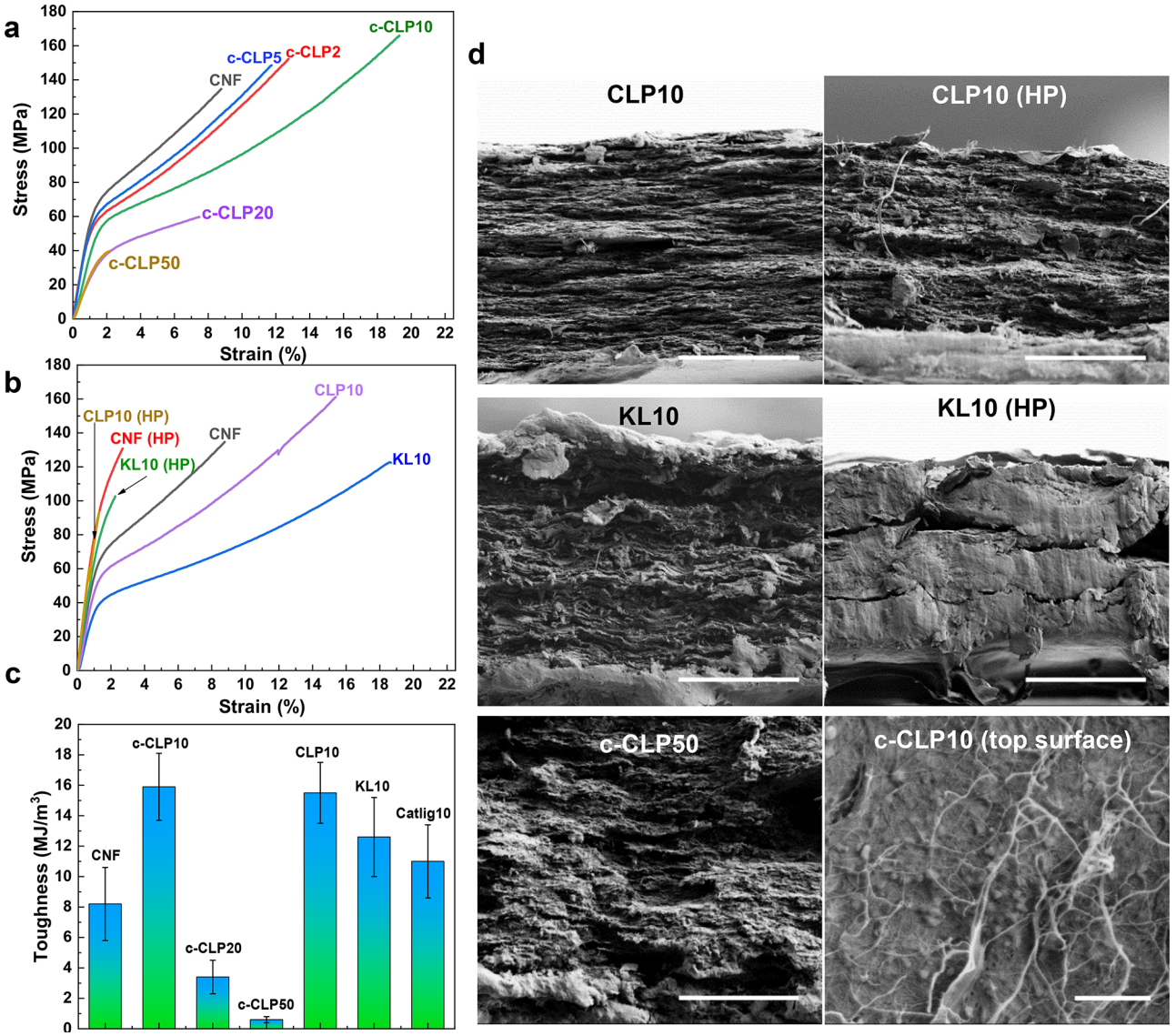

Figure 1. Mechanical properties and FESEM micrographas of lignin−CNF nanocomposites films. (a) Tensile stress−strain curves of pure CNF film and nanocomposite films with cationic colloidal lignin particles (c-CLP) at Catlig to CLPs ratio of 150 mg/g. Representative stress−strain curves, with the lowest difference in tensile stress, modulus, and strain values with respect to the mean values are shown. (b) Effect of hot pressing (HP) on tensile stress−strain curves of CNF film and nanocomposite films at 10 wt % loading of colloidal lignin particles (CLP10) and Kraft lignin (KL10). (c) Film toughness. The error bars represent ± one standard deviation from the mean. Results of statistical analysis (ANOVA) of the toughness values are shown in Table S5. (d) FESEM micrographs of the fractured cross-sectional surfaces of nanocomposite films at 10 wt % loading of colloidal lignin particles (CLP10, CLP10 (HP)), Kraft lignin (KL10, KL10 (HP)), and 50 wt % loading of cationic colloidal lignin particles (c-CLP50). Scale bars: 30 μm (cross-section) and 1 μm (top surface).

composite porosity, strength, and water interactions by altering the charge and content of CLPs in films.

Characterization of CLPs. Colloidal lignin particles termed CLPs are spherical lignin particles prepared through solvent exchange process with a few modifications.[25] In this study, acetone was used as solvent instead of tetrahydrofuran. The prepared CLPs had a Z-average diameter of 102 nm with PDI of 0.22. The ζ-potential value recorded for CLPs at pH 4.3 was −25.4 mV (Table S3). The cationic colloidal lignin particles (c-CLP) were prepared by adsorbing cationic lignin from solution on CLPs.[17] The characteristics of c-CLP prepared at different cationic lignin to CLPs ratios are tabulated in Table S3. TEM images of CLPs and c-CLP are presented in Scheme 1.

Tensile Properties of Nanocomposites. A comparative investigation of tensile properties of lignin−CNF nanocomposites comprising of different lignin morphologies, surface charge, concentration and processing conditions (Table S1) was carried out; see Figure 1a−d and the corresponding data in Table S4. We envisioned that c-CLPs would be most beneficial for the composite strength; hence, the cationicity of the particles was systematically varied. Addition of cationic colloidal lignin particles (c-CLP) with Catlig/CLP ratio of 150 mg g^{-1} increased tensile strength and strain at break compared to the corresponding values of the CNF film already at the minimum loading of 2 wt % in CNF films (Figure 1a). At an optimum 10 wt % loading of c-CLPs, the nanocomposite film demonstrated a tensile strength of 160 MPa, a clear increase from 132 MPa measured for the pure

DOI: 10.1021/acs.biomac.8b01364
Biomacromolecules 2019, 20, 693−704

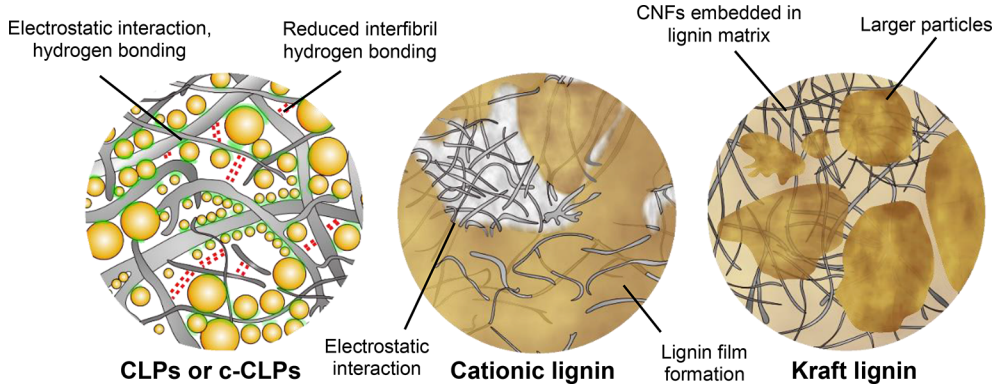

Figure 2. Schematic illustration of proposed interaction between CNF and different lignin morphologies. Note: Image is not drawn to scale.

CNF film. Importantly, this increase in tensile strength was associated with an increment of strain at break from 9.4% to 16.2%. The combination of higher elongation at break and increased tensile strength in 10 wt % c-CLP nanocomposite film led to a film structure with nearly double the toughness value (15.9 MJ m^{-3}) compared to that of the pure CNF film (8.2 MJ m^{-3}; Figure 1c). Moreover, there was no significant reduction in Young's modulus at 10 wt % CLP or c-CLP concentration (Table S4).

The ratio of cationic lignin to CLPs was altered from 50 to 300 mg g^{-1} in the preparation of c-CLPs for nanocomposite films with 10 wt % of lignin particles. However, only subtle differences in mechanical properties were observed (Table S4). A possible explanation could be the low surface charge of CNF used in this work. Instead of investigating electrostatic interactions more in detail, we decided to focus on exploring the effect of lignin morphology at 10 wt % loading. The nanocomposite film that contained 10 wt % regular CLPs exhibited similar toughness as the one with equal amount of c-CLPs, despite the opposite charge (Figure 1b). In contrast, the film with fully soluble Catlig10 exhibited weaker mechanical properties (Table S4). The KL nanocomposite film, which contains weakly anionic and irregular lignin fragments prone to aggregation, showed lower strength and toughness compared to the nanofilms containing CLPs or c-CLPs (Figure 1b).

Both CLPs and c-CLPs dispersed well and were evenly embedded in the CNF fibril network (Figure 1d), suggesting that during the film formation they restrict fibrillar entanglement, leading to even film structure with fewer aggregates (Figure S1). The presence of surface active colloidal lignin particles[17] can be correlated to the effect of lubricating polymers like poly(ethylene glycol) grafted carboxymethyl cellulose on CNF composites[26] that has a positive effect on the toughness of the nanocomposite. Furthermore, once dried, the lignin spheres will slightly disrupt the interfibrillar hydrogen bonding; however, accessible hydroxyl groups present on the surface of the CLPs can still bind to the CNF. We suggest that at the optimum CLP content of 10 wt %, both c-CLPs and unmodified CLPs act as ball bearing lubricating agents that can transfer stress and consequently enhance ductility and toughness in the composite (Figure 2). In contrast, at 50 wt % loading of c-CLPs, the fibril layer structure becomes distorted due to the high CLP content (Figure 1d). Probably the disruption in interfibrillar bonding is too severe leading to poor mechanical properties of c-CLP50 composites. FESEM micrographs (Figure S1) of fractured nanocomposite films validates increasing amount of fibril pullout (sliding) with increasing amount of CLPs in the network. At the optimum loading of CLPs (10 wt %) both fibril pullout and fibril breakage occurs. The presence of CLPs disrupts the interfibrillar hydrogen bonding pattern but are still able to form hydrogen bonds with the cellulose fibrils, hence, the strength of the film remains high.

The soluble Catlig binds well to CNF and the layered structure is very similar to the structure of pure CNF films (Figure S1). We hypothesize that this binding between Catlig and CNF is representative of a typical cationic polyelectrolyte and does not have the same stress-transferring effect as the solid particles. However, despite some apparent lignin film formation, ductility of the Catlig−CNF composite was still rather good so probably lignin as such has a positive effect.

Many earlier studies have reported detrimental effect of supplemented lignin on mechanical strength of composites, as reviewed recently.[5] It is therefore quite extraordinary that among our nanocomposite films, the film prepared by incorporating Kraft lignin (KL10) was the most ductile one, with the maximum strain at failure value of 17.8% (±2.1%), surpassing not only the values obtained in this study with colloidal lignin but also the values reported in earlier literature.[10−13,20] The Kraft lignin-containing composites (KL10) had a lower tensile strength and toughness compared to the samples containing spherical lignin particles (Figure 1b). From Figure 1d it is clear that KL forms a coating on the surface of the film. The fibril layer structure is preserved; however, the thickness of the fibril layers appears larger than those in films containing CLPs. It is postulated that CNF fibrils are embedded within the finely dispersed film-forming lignin matrix whereas large aggregates disrupt the layer packing. Recent publications have mainly studied the effect of residual lignin on the properties of CNF films. CNF nanocomposite films prepared at different residual lignin content have displayed widely distributed strain at failure values. For instance, Herrera et al.[12] obtained a maximum strain at failure value of 3.87% at a lignin content of 23%,[12] while Rojo et al.[11] and Wang et al.[10] report maximum strain values of 3.5% and 14%, at residual lignin contents of 1.7 and 5.8 wt %, respectively. However, it is difficult to conclude from these prior studies how lignin that is bound to CNF affects the strength properties. One reason for this is the poor control over spatial localization of lignin and modification of lignin for instance during sulfur dioxide pretreatment of wood[11] or alkaline sodium hypochlorite bleaching of pulp fibers.[12] The incorporation of Kraft lignin in CNF nanocomposite film preparation is scarce. However, in a recent study Liu

DOI: 10.1021/acs.biomac.8b01364
Biomacromolecules 2019, 20, 693−704

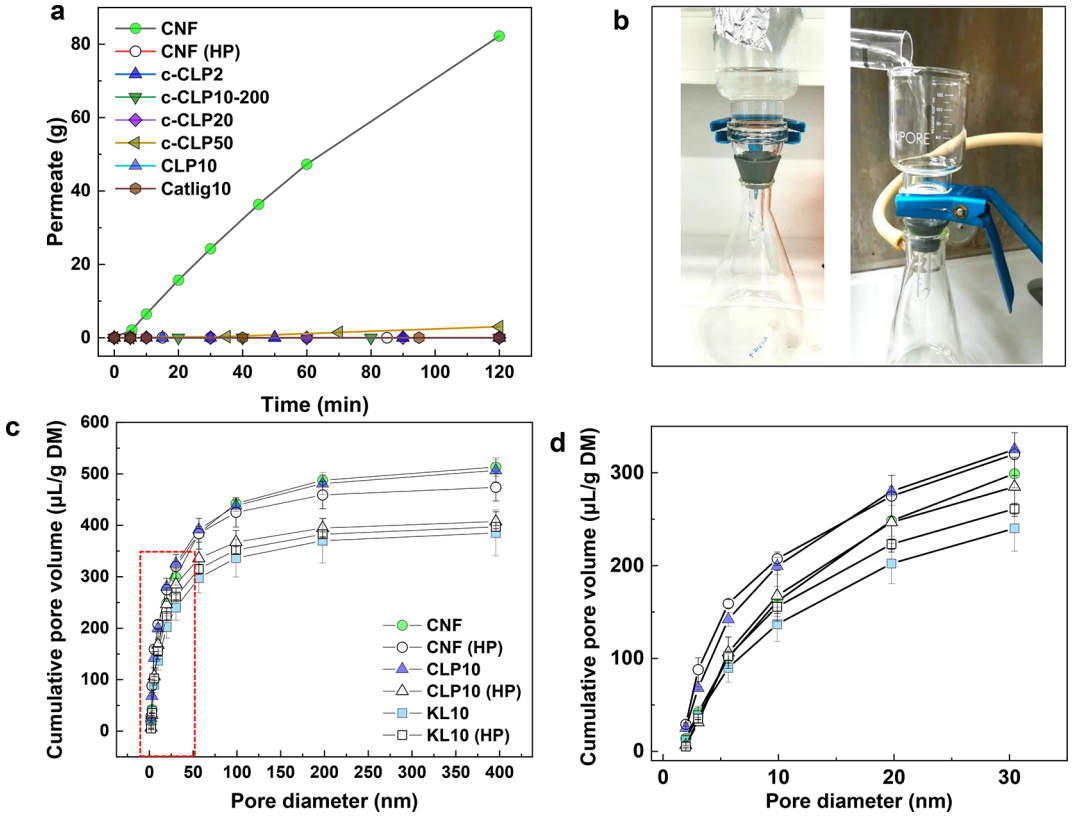

Figure 3. Effect of hot pressing and lignin content of different morphologies on water permeation and porosity of CNF film and lignin-containing CNF nanocomposite films (a) Permeation of water under ambient pressure and at room temperature. (b) Digital photographs of the water permeation experiments under ambient pressure and suction filtration. (c) Cumulative pore size distribution based on tp-DSC, red square highlights the mesoporous region. (d) Magnified view of the cumulative pore volume in the mesoporous region.

impregnated CNF with dissolved Kraft lignin or lignosulfonates and found concentration-dependent improvement with a maximum strain at failure of around 15% at 7.7% lignin content.[20] However, in those experiments, lignin-containing CNF films exhibited similar strain at failure values as the reference CNF film. The key contribution of our work is the use of separately prepared lignin dispersions in the CNF matrix that allowed us to elucidate the impact of lignin content and morphology on the mechanical properties of CNF films. In addition to understanding the lubricating effect of lignin, another interesting observation in our study was made regarding the differences between films dried upon hot pressing or under ambient conditions.

Hot pressing has been shown to increase the stress at break of CNF nanofilms.[1] With the purpose of comparing the effect of hot pressing on the mechanical properties, a hot-pressed CNF film alongside with hot-pressed CLP10 and KL10 nanocomposite films were prepared. In general, hot pressing immensely reduced the strain at failure and enhanced the Young's modulus of the films (Figure 1b). KL10 nanocomposites demonstrated drastic difference in their respective morphology upon hot pressing in comparison to ambient dried KL10 nanocomposite. The FESEM cross-section micrograph of hot pressed KL10 film revealed that the porous character and fibril layer structure predominantly diminished upon hot pressing (Figure 1d). The presence of fibril layer structure and porous nature enables moisture access to the fibril layers, playing a role of plasticizer during extension, resulting in ductility.[27] Compression applied during the hot pressing forces Kraft lignin particles to form a matrix phase that demolishes the porous nature of CNF network and completely covers the fibril network. Reduction in strain at failure is likely the outcome of new hydrogen bonds created during the hot pressing,[1] while at the same time restricting the interfibrillar sliding, thus, causing an increase in Young's modulus, but reduction of tensile strength.

Water Interactions of Nanocomposite Films. Water plays a central role in all biomaterials, and the nature of water and its mobility attract renewed interest in various engineering and science fields.[27−29] Water resistant films are in great demand in biodegradable food packaging, and in turn, the ability to control porosity and consequently water permeability by spherical lignin particles of either anionic or cationic surface charge holds many possibilities to tailor functionality of the nanofilms. We were interested in water interactions of lignin-containing CNF films also from the fundamental viewpoint. To gain insight into the wetting behavior, we first determined water contact angles (WCA) of various CNF nanocomposite films, but found them highly hydrophilic with WCA < 10°. Despite such high hydrophilicity, the nanocomposite films revealed remarkable impermeability to water that prompted our interest to investigate their moisture sorption capacities and porosities at the nanoscale.

Water Permeability. To evaluate the resistance of CNF film and lignin-containing CNF nanocomposite films against water permeation, we carried out ambient and vacuum assisted filtration tests. As expected, CNF film allowed water to permeate through the film at ambient pressure and under vacuum (Figure 3a and Table S6). However, hot-pressed CNF film resisted water permeation in both filtration conditions.

DOI: 10.1021/acs.biomac.8b01364
Biomacromolecules 2019, 20, 693−704

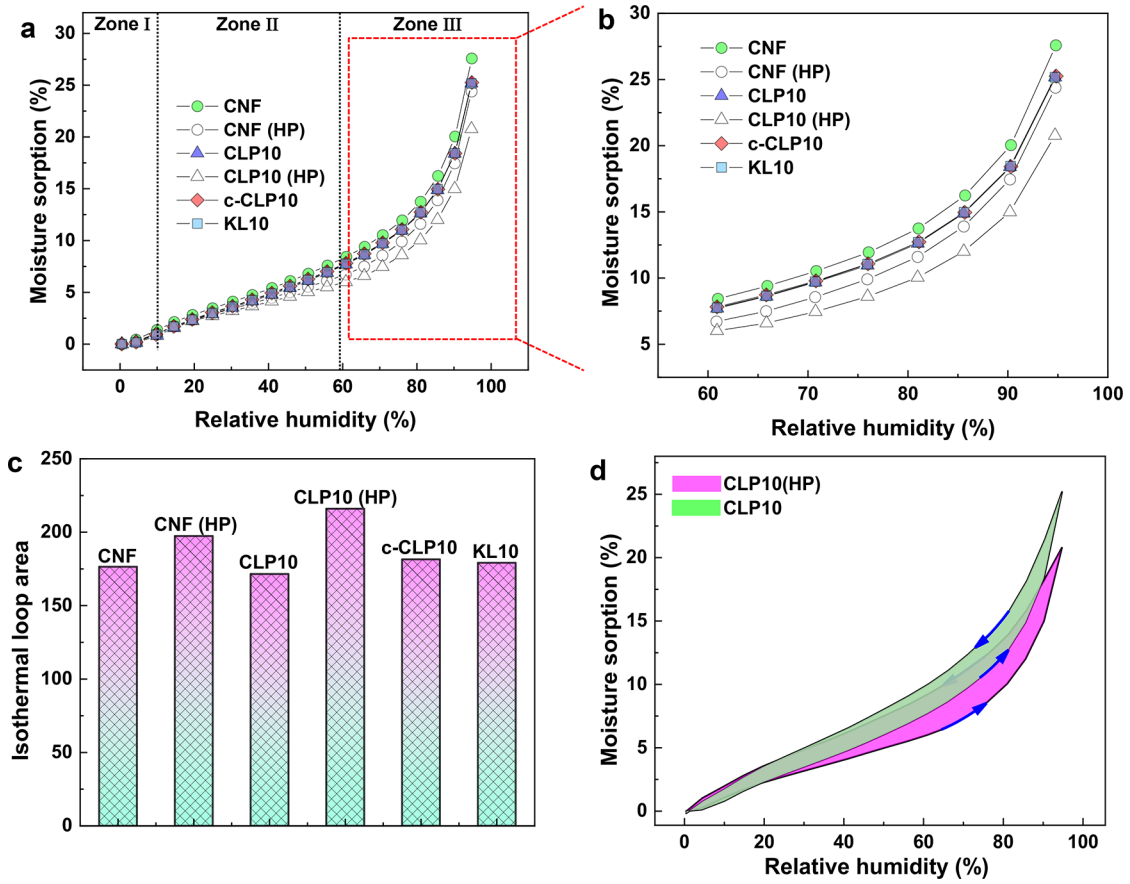

Figure 4. Moisture sorption as a function of relative humidity. (a) Sorption isotherms for CNF and lignin−CNF nanocomposite films as a function of relative humidity. (b) Magnified view of the sorption isotherms from 60 to 95% RH. (c) Comparison of mathematical area of the isotherm loop. (d) Sorption isotherm loops of CLP10 and CLP10 (HP).

This waterproofness due to hot pressing is known[30] and can be associated with the decrease in porosity and higher amount of interfibrillar bonds created due to the drying under elevated temperature and pressure. It is postulated that, in the presence of water molecules in larger pores, interactions between fibrils and water is more dominant. Drying at elevated temperature and pressure causes a reduction in water bearing larger pores as revealed by tp-DSC (Figure 3c). Consequently, stronger interfibril interaction results from the overall reduction in cumulative pore volume.

Water permeation of lignin-containing nanocomposites dried at ambient conditions revealed interesting findings. The addition of 2 wt % of c-CLPs induced water resistance in the nanocomposite film at both ambient pressure and vacuum assisted filtration conditions. This outcome is likely a consequence of physical blocking of pores in the CNF matrix resulting in hindering the passage for water to permeate the film. CLP10 nanocomposite film also demonstrated water-proofness in the filtration tests. Comparing ambient dried CNF and CLP10 we note that their overall porosity is similar (Figure 3c), but the CLP10 sample has a higher percentage of pores in the mesoporous range (Figure 3d). This suggest a relatively larger abundance of small pores, that would exert high capillary pressure, which would restrict the water permeation through the film. Interestingly, the CLP10 film showed similar cumulative pore volumes in the mesoporous size as the hot pressed CNF sample, which may explain the similar water resistant character of hot-pressed CNF film and CLP10 ambient dried nanocomposite films. Furthermore, due to the porous nature of CLPs the ambient dried CLP10 film retains larger cumulative pore volume in the macroporous (>50 nm) region compared to the hot-pressed CNF film. It is evident from thermoporometry results that hot pressing of pure CNF and CLP10 films renders a reduction in the cumulative pore volume.

The FESEM micrograph (Figure 1d) indicated that CLPs were well dispersed in the CNF network, which would restrict the fibril aggregation, thus resulting in optimum composite structure capable of water resistance. A recent paper reported that water vapor permeability of soybean protein isolate films was reduced by 40% when either calcium lignosulfonate or Sigma-Aldrich alkali lignin was used as a filler in the film matrix.[31] In the present study, the c-CLP nanocomposite films retained their water resistant character completely until 20 wt % of lignin content. At 50 wt % c-CLP content, slight water permeation was possible either due to the uneven thickness of the film or weak interfibril interactions and entanglements caused by the presence of large amount of c-CLPs. The weaker network structure when lignin content increased beyond the optimum 10 wt % were likewise shown by the mechanical test results discussed above.

Moisture Sorption Isotherms. The effect of the different lignin morphologies on the moisture uptake of the CNF film and lignin-containing nanocomposite films was studied by dynamic vapor sorption (DVS) analysis. Moisture sorption kinetics were performed on ambient dried and hot-pressed

DOI: 10.1021/acs.biomac.8b01364
Biomacromolecules 2019, 20, 693−704

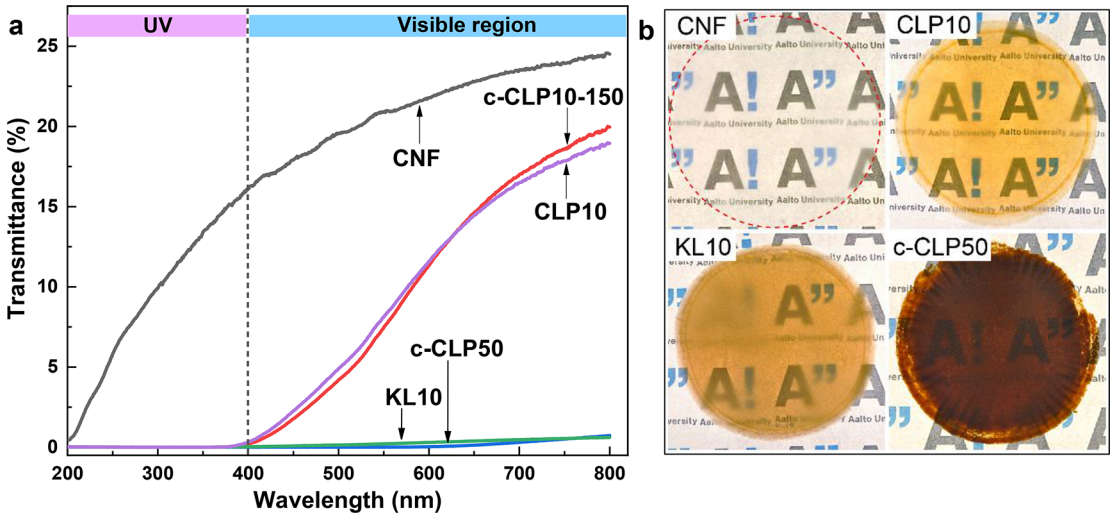

Figure 5. Optical properties of CNF and lignin CNF nanocomposite films. (a) UV−vis light transmittance spectra. (b) Digital photographs showing the optical transparency of pure CNF, c-CLP10, KL10, and c-CLP50. The logo is used with permission from Aalto University.

films of CNF film and nanocomposite films at 10 wt % lignin content. The corresponding sorption isotherms are presented in Figure 4a. Curves for all the measured samples display sigmoid or S-shape profile, in which the curves concave upward. This kind of isotherm represents the presence of multilayers of water molecules at the internal surface of a material.[32]

At low RH values (0−15%), surface of the nanocomposite films receives a monolayer of bound water, between 15−70% RH, multilayer of water molecules becomes deposited. This impregnation of water molecules forces cellulose nanofibrillar network to swell due to the reduced interfibrillar hydrogen bonding, which is also responsible for an increase in oxygen permeation.[1] As the RH increases beyond 70%, a rapid increase in the equilibrium moisture content due to the capillary condensation of water molecules in CNF film pores occurs.[32] This phenomenon is typical for cellulose whiskers and CNF network films.[33] The obtained sorption isotherms for CNF and lignin CNF nanocomposites are in close approximation to oxygen transmission rate (OTR) measurement as a function of RH, mainly due to their moisture-sensitive nature.[1]

The tested films of pure CNF and nanocomposites displayed marginal differences in their respective sorption isotherms until 50% RH; however, upon further increasing of the RH, there is a clear difference in the moisture sorption behaviors. At the maximum RH of 95%, hot-pressed nanocomposite films demonstrated lower water sorption compared to the ambient-dried ones (Figure 4b). Ambient-dried CNF film reached an equilibrium moisture content (EMC) of 27.6%, while the hot pressed CNF film exhibited an EMC of 24.4%. Similarly, ambient dried CLP10 nanocomposite films showed an EMC of 25.2% compared to 20.8% for the hot pressed CLP10 film. The reduction in the EMC of hot pressed films can be attributed to the stiffer interfibrillar matrix and loss in cumulative pore volume as shown by tp-DSC (Figure 3c).

It is interesting to note that at the moisture content values of 95% RH, the ambient dried nanocomposites at 10 wt % of lignin content showed similar moisture sorption as the hot-pressed CNF film complementing the aforementioned water permeation results (Figure 3a). In addition, among the ambient-dried lignin-containing nanocomposites films, c-CLP10 and CLP10, displayed identical sorption isotherms, and EMC values, ruling out the effect of opposite charge and different morphological structure on sorption behavior. KL10 nanocomposite also demonstrated similar moisture sorption as c-CLP10 and CLP10, indicating that at 10 wt % of lignin content the moisture sorption of nanocomposites prepared under similar condition remains unaffected by the morphology of the lignin.

The sorption hysteresis is directly associated with the adsorption and desorption of water molecules in and out of the matrix, causing deformation.[34,35] The difference between the sorption and adsorption curves forms hysteresis, which is associated with the nature and ability of a material for conformational and structural rearrangements.[35] The sorption hysteresis of each film was further characterized by calculating the mathematical loop area of the isotherms (Figure 4c). The CLP10 (HP) showed the largest hysteresis. Comparatively, ambient-dried CLP10 nanocomposite film demonstrated the lowest total hysteresis, with the CNF film in between. The obtained results indicate that the moisture sorption capacity of ambient dried nanocomposite films is higher than the hot pressed films. During the sorption cycle, ambient dried films absorb more moisture compared to hot-pressed films whereas, during the desorption cycle, hot pressed films have higher tendency to retain the absorbed moisture in comparison to ambient dried films. (Figure 4d).

Stability in Physiological Buffer Medium. The stability of CNF−lignin nanocomposites films in simulated physiological fluid was examined by exposing them to a PBS buffer at pH 5.5. After 24 h of rotational agitation at 37 °C, absorbance spectra were collected to assess the leaching of lignin nanoparticles through the films. Nanocomposite films released only a subtle amount of lignin based on zero absorbance at visible wavelengths and low, lignin content-dependent absorbance at 280 nm (Figure S2). Nanocomposite films at 10 wt % loading of c-CLPs, CLPs, and KL demonstrated a 10-fold increment in their absorbance compared to the pure CNF film. At 50% loading of c-CLPs, the absorbance was approximately 3-fold compared to that of films with 10 wt % lignin. The film specimens remained physically intact because the leaching amounted less than 5% of lignin initially present in

DOI: 10.1021/acs.biomac.8b01364
Biomacromolecules 2019, 20, 693−704

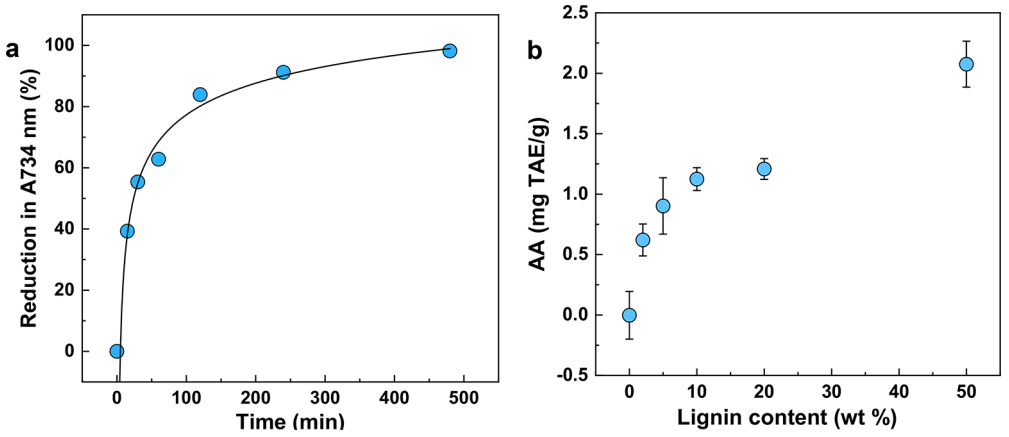

Figure 6. Antioxidant activity of lignin CNF nanocomposite films. (a) Antioxidant kinetics of the c-CLP10 (200 mg g^{-1} Catlig to CLPs) nanocomposite film. Reduction in absorbance of $ABTS^{\bullet+}$ radical cation solution at 734 nm is shown. Curve fit: $y = a\ \ln(-b \times \ln(x))$, where a = 73.90 and b = −0.618. (b) Effect of lignin content on antioxidant activity of c-CLP nanocomposite films.

the nanofilms (using arbitrary mass extinction coefficient of 25 L g^{-1} cm^{-1} for the solubilized lignin).

UV Shielding and Antioxidant Activity. The presence of phenolic rings in lignin are known to give antioxidant and anti-UV properties.[36] To analyze the UV-shielding potential of lignin-containing nanocomposite films, UV−vis transmittance spectra of CNF, c-CLP10, c-CLP50, CLP10, and KL10 are compared in Figure 5a.

The lignin-CNF nanocomposite films expectedly demonstrated suppression of transmittance of UV light. Independent of lignin type and concentration, nanocomposite films revealed strong absorption for both UV-B (280−315 nm) and UV-A (315−400 nm) regions, compared to the weaker performance of the CNF film (Figure 5a). The transmittance values of the lignin-containing films are close to zero over the entire UV wavelength range 200−400 nm. In the visible light region (400−800 nm), the c-CLP nanocomposites films showed concentration-dependent optical transmittance. With increasing lignin concentration, the color of the c-CLP nanocomposite films turns darker causing lower optical transmittance compared to the pure CNF film as shown in Figure 5b and Figure S3. The nanocomposite film at 10 wt % loading of c-CLPs maintained a transmittance of 18.6%, whereas c-CLP loading of 50 wt % permitted transmittance of only 0.5%. The opacity of the films increased considerably with increasing c-CLP content. Decrease in the visible light transmittance in c-CLP50 nanocomposite film is associated with the increased content of cationic colloidal lignin nanoparticles causing higher absorbance of visible light. Furthermore, the increase in the dispersed phase in the nanocomposite films at higher loading of c-CLPs evokes scattering. The optical transmittance of CLP10 nanocomposite film is similar to c-CLP10 nanocomposites films having a transmittance value of 17.8% at 748 nm, however at similar lignin content the Kraft lignin nanocomposite film (KL10) demonstrated transmittance of only 0.5%. This drop in transmittance is due to the larger particle size (DLS and FESEM results in Table S3 and Figure S1), causing light scattering from the KL10 film. Obtained transmittance data suggests that upon the addition of lignin, c-CLP, and CLP, but not KL, provide an efficient UV shielding capability in CNF nanocomposite films, with only moderate sacrifice in visible light transparency.

Antioxidant Activity. The free radical scavenging activity of lignin and other polyphenolics makes them useful sources of antioxidant compounds.[5] Due to the presence of aromatic rings with methoxy and hydroxyl functional groups within lignin structure, the propagation of oxidation reactions can be terminated through hydrogen donation.[37,38] The vast majority of earlier studies have used the DPPH antioxidant assay involving contacting soluble or solid material with DPPH radical in ethanol or methanol.[31,39−42] These alcohols are relatively good solvents for lignin, especially the low molecular weight fragments. Effectively, the tests have shown more the antioxidant activity of the migrating substances than the material that remains in the insoluble matrix.[40,43] Further, the solvent medium is unnatural when compared to any expectable environment in food packaging or biomedical applications. We therefore modified the $ABTS^{\bullet+}$ radical scavenging assay, which allows reactions in aqueous medium, by using a longer reaction time of 60 min compared to the regular 1 min used in the original method.[24] We reasoned that these conditions are better suited to the analysis of films and solid materials in general.

The kinetics of the antioxidant test with a typical nanocomposite film (CNF with 20 wt % c-CLPs) is shown in Figure 6a. From these results, it is evident that the antioxidant activity increases rapidly within the first 100 min, and thereafter slowly plateaus due to the exhaustion of the available concentration of $ABTS^{\bullet+}$ radical cation. The antioxidant activity as a function of c-CLP loading in lignin CNF nanocomposites is shown in Figure 6b. The nanocomposite films demonstrated an increase in the antioxidant activity with the increasing content of c-CLP, as could be expected from the known antioxidant activity of lignin nanoparticles.[40,44−46] The antioxidant activity of CNF film is around zero and increases from 0.62 mg TAE g^{-1} at the minimum lignin content of 2 wt % to 1.21 mg TAE g^{-1} at 10 wt % and further to 2.07 mg g^{-1} at 50 wt % of c-CLPs. The observed nonlinear correlation is probably due to the increasing diffusion barrier, as the lignin content and film thickness increase. The absolute antioxidant values of 1−2 mg TAE g^{-1} film are lower compared to reported values of 15−28 mg ascorbic acid g^{-1} fully solubilized gelatin films that contained 15 wt % of grass soda lignin.[41] However, contrary to the soluble lignin−gelatin films, our films were essentially fully insoluble in aqueous media, maintaining the radical scavenging activity in the solid matrix.

DOI: 10.1021/acs.biomac.8b01364
Biomacromolecules 2019, 20, 693−704

To further explore the effect of cationic lignin coating on the CLP surface, the nanocomposite films prepared at 10 wt % CLP loading, with Catlig/CLPs ratio of 50, 100, 200, and 300 mg/g were also investigated. The antioxidant activity data acquired implies that the Catlig/CLP ratio had only a moderate effect on increasing the antioxidant activity. Therefore, the excess of Catlig that was not bound to CLPs was probably sterically hindered in the CNF network (Figure S4). Despite the contrastive particle sizes and morphologies, similar antioxidant capacities were obtained with CLP, Catlig and KL at 10 wt % loading (Figure S5). Put together, these results suggest that the antioxidant action occurred mainly at the liquid−solid interface.

CONCLUSIONS

In the present study, cellulose nanofibril nanocomposite films utilizing a variety of different lignin morphologies were prepared using a pressurized filtration method. Tensile measurements revealed a significant improvement in the mechanical properties of nanocomposite films that contained colloidal lignin particles. At 10 wt % content of either regular or cationic lignin particles, tensile strength of nanocomposite film reached 160 MPa along with a strain at break value of 16%. The resulting lignin-containing nanocomposite films showed nearly double the toughness of CNF film. Observed water impermeability in conjunction with the investigation of water sorption, microstructure, and nanoscaled porosity of the composite films suggested that spherical lignin nanoparticles acted as lubricating and stress transferring agents, explaining the increase in toughness and ductility of the CNF composites. Furthermore, nanocomposite films containing colloidal lignin particles blocked UV light, while maintaining a higher visible light transmittance than the films that contained irregular lignin aggregates instead of nanoparticles. Moreover, lignin particles delivered a long lasting radical scavenging activity that might be useful in packaging and healthcare applications. Overall, our work demonstrated that colloidal lignin particles provide multifunctional properties to nanocomposites, encouraging renewed efforts to develop innovative materials solely from natural lignocellulosic biopolymers.

ASSOCIATED CONTENT

Supporting Information

The Supporting Information is available free of charge on the ACS Publications website at DOI: 10.1021/acs.biomac.8b01364.

Additional FESEM micrographs of the surface and cross-section of pure CNF and lignin−CNF nanocomposite films (Figure S1); Absorbance of aqueous buffer solution after 24 h contact with the nanofilms under simulated physiological conditions at 280 nm (Figure S2); Digital photographs of the CNF nanofilm and CNF−lignin nanofilms (Figure S3); Antioxidant activity as a function of Catlig/CLPs ratio (Figure S4); Effect of different lignin morphologies at 10 wt % of lignin content on antioxidant activity (Figure S5); Weight percent (w/w) composition and mass balance closure CNF film and nanocomposite films (Table S1); The tp-DSC temperature program (Table S2); Particle size distribution and ζ-potentials of lignin materials (Table S3); Physical and mechanical properties for CNF and CNF/lignin composite films (Table S4); Statistical analysis of toughness values of CNF film and CNF−lignin nanocomposite films (Table S5); Water permeability data of CNF and CNF−lignin nanofilms (Table S6) (DOCX).
Video S1: CNF film ambient filtration test (AVI).
Video S2: CNF film suction filtration test (AVI).
Video S3: c-CLP2 suction filtration test (AVI).
Video S4: CLP10 suction filtration test (AVI).
Video S5: Suction filtration test without nanofilm (AVI).

AUTHOR INFORMATION

Corresponding Authors

*E-mail: mika.sipponen@aalto.fi. Phone: +358503013978.
*E-mail: monika.osterberg@aalto.fi. Phone: +358505497218.

ORCID

Mika H. Sipponen: 0000-0001-7747-9310
Monika Österberg: 0000-0002-3558-9172

Author Contributions

M.F. designed the experiments with T.Z., M.H.S., and M.Ö. Experiments and data analysis was performed by M.F. in collaboration with M.H.S, and M.Ö. T.Z. contributed to the sample preparation and optimization. G.R conducted the spectrophotometric transmittance measurements and antioxidant characterization. M.F wrote the manuscript with input from all authors. All authors discussed the results, read and approved the manuscript.

Notes

The authors declare no competing financial interest.

ACKNOWLEDGMENTS

The authors have filed a provisional patent application related to the results presented herein. Authors acknowledge Dr. Michael Altgen and Dr. Eeva-Leena Rautama for technical assistance, and M.Sc. Eija-Katriina Uusi-Tarkka for preliminary experiments. M.H.S. and M.Ö. acknowledge Academy of Finland for funding (Grants 296547 and 278279, respectively). G.R. acknowledges Zelcor Project and funding from Bio-Based Industries Joint Undertaking under the European Union's Horizon 2020 research and innovation program (Grant Agreement No. 720303). T.Z. acknowledges funding from the Novo Nordisk Foundation (SUSCELL project, Reference Number: NNF17OC0027658). The work was part of the Academy of Finland Flagship's programme under projects No. 318890 and 318891 (Competence Center for Materials Bioeconomy, FinnCERES).

REFERENCES

(1) Österberg, M.; Vartiainen, J.; Lucenius, J.; Hippi, U.; Seppälä, J.; Laine, J. A Fast Method to Produce String NFC Films as a Platform for Barrier and Functional Materials. *ACS Appl. Mater. Interfaces* **2013**, *5*, 4640−4647.
(2) Toivonen, M. S.; Kurki-Suonio, S.; Schacher, F. H.; Hietala, S.; Rojas, O. J.; Ikkala, O. Water-Resistant, Transparent Hybrid Nanopaper by Physical Cross-Linking with Chitosan. *Biomacromolecules* **2015**, *16*, 1062−1071.
(3) Wen, J. L.; Xue, B. L.; Xu, F.; Sun, R. C. Unveiling the Structural Heterogeneity of Bamboo Lignin by In Situ HSQC NMR Technique. *BioEnergy Res.* **2012**, *5*, 886−903.
(4) Thulluri, C.; Pinnamaneni, S. R.; Shetty, P. R.; Addepally, U. Synthesis of Lignin-Based Nanomaterials/Nanocomposites: Recent Trends and Future Perspectives. *Ind. Biotechnol.* **2016**, *12*, 153−160.
(5) Kai, D.; Tan, M. J.; Chee, P. L.; Chua, Y. K.; Yap, Y. L.; Loh, X. J. Towards Lignin-Based Functional Materials in a Sustainable World. *Green Chem.* **2016**, *18*, 1175−1200.

DOI: 10.1021/acs.biomac.8b01364
Biomacromolecules 2019, 20, 693−704

(6) Fratzl, P.; Weinkamer, R. Nature's Hierarchical Materials. *Prog. Mater. Sci.* **2007**, *52*, 1263−1334.
(7) Laschimke, R. Investigation of the Wetting Behaviour of Natural Lignin - a Contribution to the Cohesion Theory of Water Transport in Plants. *Thermochim. Acta* **1989**, *151*, 35−56.
(8) Henriksson, M.; Berglund, L. A.; Isaksson, P.; Lindström, T.; Nishino, T. Cellulose Nanopaper Structures of High Toughness. *Biomacromolecules* **2008**, *9*, 1579−1585.
(9) Shimizu, M.; Saito, T.; Fukuzumi, H.; Isogai, A. Hydrophobic, Ductile, and Transparent Nanocellulose Films with Quaternary Alkylammonium Carboxylates on Nanofibril Surfaces. *Biomacromolecules* **2014**, *15*, 4320−4325.
(10) Wang, Q.; Du, H.; Zhang, F.; Zhang, Y.; Wu, M.; Yu, G.; Liu, C.; Li, B.; Peng, H. Flexible Cellulose Nanopaper with High Wet Tensile Strength, High Toughness and Tunable Ultraviolet Blocking Ability Fabricated from Tobacco Stalk: Via a Sustainable Method. *J. Mater. Chem. A* **2018**, *6*, 13021−13030.
(11) Rojo, E.; Peresin, M. S.; Sampson, W. W.; Hoeger, I. C.; Vartiainen, J.; Laine, J.; Rojas, O. J. Comprehensive Elucidation of the Effect of Residual Lignin on the Physical, Barrier, Mechanical and Surface Properties of Nanocellulose Films. *Green Chem.* **2015**, *17*, 1853−1866.
(12) Herrera, M.; Thitiwutthisakul, K.; Yang, X.; Rujitanaroj, P. on; Rojas, R.; Berglund, L. Preparation and Evaluation of High-Lignin Content Cellulose Nanofibrils from Eucalyptus Pulp. *Cellulose* **2018**, *25*, 3121−3133.
(13) Bian, H.; Gao, Y.; Wang, R.; Liu, Z.; Wu, W.; Dai, H. Contribution of Lignin to the Surface Structure and Physical Performance of Cellulose Nanofibrils Film. *Cellulose* **2018**, *25*, 1309−1318.
(14) Peresin, M. S.; Vesterinen, A. H.; Habibi, Y.; Johansson, L. S.; Pawlak, J. J.; Nevzorov, A. A.; Rojas, O. J. Crosslinked PVA Nanofibers Reinforced with Cellulose Nanocrystals: Water Interactions and Thermomechanical Properties. *J. Appl. Polym. Sci.* **2014**, *131*, 1−12.
(15) Lintinen, K.; Xiao, Y.; Bangalore Ashok, R. P.; Leskinen, T.; Sakarinen, E.; Sipponen, M. H.; Farooq, M.; Oinas, P.; Österberg, M.; Kostiainen, M. A. Closed Cycle Production of Concentrated and Dry Redispersible Colloidal Lignin Particles with a Three Solvent Polarity Exchange Method. *Green Chem.* **2018**, *20*, 843−850.
(16) Sipponen, M. H.; Farooq, M.; Koivisto, J.; Pellis, A.; Seitsonen, J.; Österberg, M. Spatially Confined Lignin Nanospheres for Biocatalytic Ester Synthesis in Aqueous Media. *Nat. Commun.* **2018**, *9*, 1−7.
(17) Sipponen, M. H.; Smyth, M.; Leskinen, T.; Johansson, L. S.; Österberg, M. All-Lignin Approach to Prepare Cationic Colloidal Lignin Particles: Stabilization of Durable Pickering Emulsions. *Green Chem.* **2017**, *19*, 5831−5840.
(18) Qian, Y.; Qiu, X.; Zhu, S. Lignin: A Nature-Inspired Sun Blocker for Broad-Spectrum Sunscreens. *Green Chem.* **2015**, *17*, 320−324.
(19) Tardy, B. L.; Richardson, J. J.; Guo, J.; Lehtonen, J.; Ago, M.; Rojas, O. J. Lignin Nano- and Microparticles as Template for Nanostructured Materials: Formation of Hollow Metal-Phenolic Capsules. *Green Chem.* **2018**, *20*, 1335−1344.
(20) Liu, Y. Strong and Flexible Nanocomposites of Carboxylated Cellulose Nanofibril Dispersed by Industrial Lignin. *ACS Sustainable Chem. Eng.* **2018**, *6*, 5524−5532.
(21) Eronen, P.; Laine, J.; Ruokolainen, J.; Österberg, M. Comparison of Multilayer Formation Between Different Cellulose Nanofibrils and Cationic Polymers. *J. Colloid Interface Sci.* **2012**, *373*, 84−93.
(22) Park, S.; Venditti, R. A.; Jameel, H.; Pawlak, J. J. Changes in Pore Size Distribution during the Drying of Cellulose Fibers as Measured by Differential Scanning Calorimetry. *Carbohydr. Polym.* **2006**, *66*, 97−103.
(23) Pihlajaniemi, V.; Sipponen, M. H.; Liimatainen, H.; Sirviö, J. A.; Nyyssölä, A.; Laakso, S. Weighing the Factors behind Enzymatic Hydrolyzability of Pretreated Lignocellulose. *Green Chem.* **2016**, *18*, 1295−1305.
(24) Re, R.; Pellegrini, N.; Proteggente, A.; Pannala, A.; Yang, M.; Rice-Evans, C. Antioxidant Activity Applying an Improved Abts Radical. *Free Radical Biol. Med.* **1999**, *26*, 1231−1237.
(25) Lievonen, M.; Valle-Delgado, J. J.; Mattinen, M. L.; Hult, E. L.; Lintinen, K.; Kostiainen, M. A.; Paananen, A.; Szilvay, G. R.; Setälä, H.; Österberg, M. A Simple Process for Lignin Nanoparticle Preparation. *Green Chem.* **2016**, *18*, 1416−1422.
(26) Olszewska, A.; Valle-Delgado, J. J.; Nikinmaa, M.; Laine, J.; Österberg, M. Direct Measurements of Non-Ionic Attraction and Nanoscaled Lubrication in Biomimetic Composites from Nanofibrillated Cellulose and Modified Carboxymethylated Cellulose. *Nanoscale* **2013**, *5*, 11837−11844.
(27) Benítez, A. J.; Torres-Rendon, J.; Poutanen, M.; Walther, A. Humidity and Multiscale Structure Govern Mechanical Properties and Deformation Modes in Films of Native Cellulose Nanofibrils. *Biomacromolecules* **2013**, *14*, 4497−4506.
(28) O'Neill, H.; Pingali, S. V.; Petridis, L.; He, J.; Mamontov, E.; Hong, L.; Urban, V.; Evans, B.; Langan, P.; Smith, J. C.; Davison, B. H. Dynamics of Water Bound to Crystalline Cellulose. *Sci. Rep.* **2017**, *7*, 1−13.
(29) Hakalahti, M.; Faustini, M.; Boissière, C.; Kontturi, E.; Tammelin, T. Interfacial Mechanisms of Water Vapor Sorption into Cellulose Nanofibril Films as Revealed by Quantitative Models. *Biomacromolecules* **2017**, *18*, 2951−2958.
(30) Kargarzadeh, H.; Ahmad, I.; Thomas, S.; Dufresne, A. *Handbook of Nanocellulose and Cellulose Nanocomposites*; John Wiley & Sons, Inc., 2017.
(31) Zadeh, E. M.; O'Keefe, S. F.; Kim, Y. T. Utilization of Lignin in Biopolymeric Packaging Films. *ACS Omega* **2018**, *3*, 7388−7398.
(32) Hill, C. A. S.; Norton, A.; Newman, G. The Water Vapor Sorption Behavior of Natural Fibers. *J. Appl. Polym. Sci.* **2009**, *112*, 1524−1537.
(33) Guo, X.; Liu, L.; Hu, Y.; Wu, Y. Water Vapor Sorption Properties of TEMPO Oxidized and Sulfuric Acid Treated Cellulose Nanocrystal Films. *Carbohydr. Polym.* **2018**, *197*, 524−530.
(34) Fredriksson, M.; Thybring, E. E. Scanning or Desorption Isotherms? Characterising Sorption Hysteresis of Wood. *Cellulose* **2018**, *25*, 4477−4485.
(35) Guo, X.; Liu, L.; Hu, Y.; Wu, Y. Water Vapor Sorption Properties of TEMPO Oxidized and Sulfuric Acid Treated Cellulose Nanocrystal Films. *Carbohydr. Polym.* **2018**, *197*, 524−530.
(36) Pouteau, C.; Dole, P.; Cathala, B.; Averous, L.; Boquillon, N. Antioxidant Properties of Lignin in Polypropylene. *Polym. Degrad. Stab.* **2003**, *81*, 9−18.
(37) Dizhbite, T.; Telysheva, G.; Jurkjane, V.; Viesturs, U. Characterization of the Radical Scavenging Activity of Lignins - Natural Antioxidants. *Bioresour. Technol.* **2004**, *95*, 309−317.
(38) Lu, F. J.; Chu, L. H.; Gau, R. J. Free Radical-Scavenging Properties of Lignin. *Nutr. Cancer* **1998**, *30*, 31−38.
(39) Crouvisier-Urion, K.; Bodart, P. R.; Winckler, P.; Raya, J.; Gougeon, R. D.; Cayot, P.; Domenek, S.; Debeaufort, F.; Karbowiak, T. Biobased Composite Films from Chitosan and Lignin: Antioxidant Activity Related to Structure and Moisture. *ACS Sustainable Chem. Eng.* **2016**, *4*, 6371−6381.
(40) Yang, W.; Owczarek, J. S.; Fortunati, E.; Kozanecki, M.; Mazzaglia, A.; Balestra, G. M.; Kenny, J. M.; Torre, L.; Puglia, D. Antioxidant and Antibacterial Lignin Nanoparticles in Polyvinyl Alcohol/Chitosan Films for Active Packaging. *Ind. Crops Prod.* **2016**, *94*, 800−811.
(41) Núñez-Flores, R.; Giménez, B.; Fernández-Martín, F.; López-Caballero, M. E.; Montero, M. P.; Gómez-Guillén, M. C. Physical and Functional Characterization of Active Fish Gelatin Films Incorporated with Lignin. *Food Hydrocolloids* **2013**, *30*, 163−172.
(42) Domenek, S.; Louaifi, A.; Guinault, A.; Baumberger, S. Potential of Lignins as Antioxidant Additive in Active Biodegradable Packaging Materials. *J. Polym. Environ.* **2013**, *21*, 692−701.

DOI: 10.1021/acs.biomac.8b01364
Biomacromolecules 2019, 20, 693−704

(43) Crouvisier-Urion, K.; Lagorce-Tachon, A.; Lauquin, C.; Winckler, P.; Tongdeesoontorn, W.; Domenek, S.; Debeaufort, F.; Karbowiak, T. Impact of the Homogenization Process on the Structure and Antioxidant Properties of Chitosan-Lignin Composite Films. *Food Chem.* **2017**, *236*, 120−126.
(44) Tian, D.; Hu, J.; Bao, J.; Chandra, R. P.; Saddler, J. N.; Lu, C. Lignin Valorization: Lignin Nanoparticles as High-Value Bio-Additive for Multifunctional Nanocomposites. *Biotechnol. Biofuels* **2017**, *10*, 1−11.
(45) Sipponen, M. H.; Lange, H.; Ago, M.; Crestini, C. Understanding Lignin Aggregation Processes. A Case Study: Budesonide Entrapment and Stimuli Controlled Release from Lignin Nanoparticles. *ACS Sustainable Chem. Eng.* **2018**, *6*, 9342−9351.
(46) Yearla, S. R.; Padmasree, K. Preparation and Characterisation of Lignin Nanoparticles: Evaluation of Their Potential as Antioxidants and UV Protectants. *J. Exp. Nanosci.* **2016**, *11*, 289−302.

DOI: 10.1021/acs.biomac.8b01364
Biomacromolecules 2019, 20, 693−704